Structural insight into Parkinson's disease treatment from drug-inhibited DOPA decarboxylase

Peter Burkhard[1], Paola Dominici[2,3], Carla Borri-Voltattorni[2], Johan N. Jansonius[4] and Vladimir N. Malashkevich[4,5]

[1]M.E. Müller Institute for Structural Biology, Biozentrum, University of Basel, Klingelbergstrasse 70, CH-4056 Basel, Switzerland. [2]Dipartimento di Scienze Neurologiche e della Visione, Sezione di Chimica Biologica, Università di Verona, Strada Le Grazie, 8, 37134 Verona, Italy. [3]Current address: Dipartimento Scientifico e Tecnologico, Università degli Studi di Verona, 37134 Verona, Italy. [4]Department of Structural Biology, Biozentrum, University of Basel, Klingelbergstrasse 70, CH-4056 Basel, Switzerland. [5]Current address: Whitehead Institute for Biomedical Research, 9 Cambridge Center, Cambridge, Massachusetts 02142, USA.

DOPA decarboxylase (DDC) is responsible for the synthesis of the key neurotransmitters dopamine and serotonin *via* decarboxylation of L-3,4-dihydroxyphenylalanine (L-DOPA) and L-5-hydroxytryptophan, respectively. DDC has been implicated in a number of clinic disorders, including Parkinson's disease and hypertension. Peripheral inhibitors of DDC are currently used to treat these diseases. We present the crystal structures of ligand-free DDC and its complex with the anti-Parkinson drug carbiDOPA. The inhibitor is bound to the enzyme by forming a hydrazone linkage with the cofactor, and its catechol ring is deeply buried in the active site cleft. The structures provide the molecular basis for the development of new inhibitors of DDC with better pharmacological characteristics.

Parkinson's disease (PD) is a chronic, progressive neurological disorder characterized by tremor, bradykinesia, rigidity and postural instability. Although its exact cause is not yet known, PD is thought to be the result of degeneration of dopamine-producing cells in the substantia nigra of the brain[1–3]. Human cells synthesize endogenous dopamine from L-3,4-dihydroxyphenylalanine (L-DOPA, also called levodopa) (Fig. 1), which is derived from dietary tyrosine. The conversion of L-DOPA into dopamine is catalyzed by the vitamin B_6-dependent enzyme aromatic amino acid decarboxylase, also called DOPA decarboxylase (DDC, EC 4.1.1.28), which is abundant in the nervous system and the kidney[4]. Externally supplemented L-DOPA is rapidly converted to dopamine; therefore, administration of L-DOPA remains the most effective symptomatic treatment for PD[5].

Dopamine itself, however, cannot pass the blood-brain barrier and, thus, cannot be utilized as a drug in the treatment of PD[6]. However, administration of dietary L-DOPA bypasses the rate-limiting step in dopamine biosynthesis and increases the amount of synthesized dopamine in the nerve cell. Newly synthesized dopamine is stored in granulae in the dopaminergic nerve terminals and is released into the synapse following electric stimulation from the axon. PD is accompanied by a gradual loss of the number of dopaminergic nerve cells[7]. In order to sustain its function, the brain compensates for this in part by developing new synaptic contacts on remaining neurons ('sprouting')[8] and also by increasing the sensitivity and number of dopamine receptor cells, creating supersensitivity. These mechanisms are most likely the explanation for the very good results of treatment with L-DOPA.

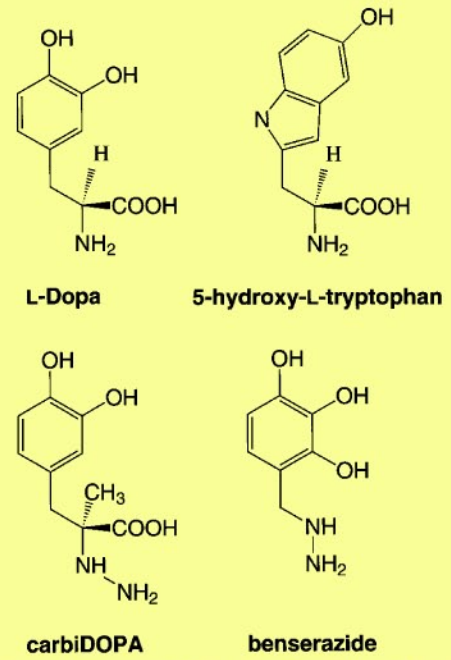

Fig. 1 The chemical structures of the substrates L-DOPA and 5-hydroxy-tryptophan and the inhibitors carbiDOPA and benserazide (in its cleaved form).

Because L-DOPA is rapidly converted to dopamine in the blood stream when administered as a drug, only a small percentage of a given dose will reach the nervous system. By adding a DDC inhibitor, as is the case in the most commonly used L-DOPA products carbiDOPA[9] or benserazide[10] (Fig. 1), greater amounts of L-DOPA can reach the brain, causing the level of dopamine there to be substantially increased. Simultaneously, dopamine-related side effects (nausea, daytime sleepiness, orthostatic hypotension, involuntary movements, decreased appetite, insomnia and cramping) and side effects due to a high concentration of L-DOPA in the blood stream are diminished. Here we present the crystal structures of pig kindey DDC alone and in complex with carbiDOPA at 2.6 and 2.25 Å resolution, respectively. These structures reveal the mode of binding of the inhibitor and suggest ways to design even more specific DDC inhibitors, which might be of great benefit to patients suffering from PD and possibly other neurological diseases.

Overall topology

We determined the three-dimensional structure of DDC in its ligand-free form and in complex with the anti-Parkinson drug carbiDOPA (Tables 1, 2; ref. 11). DDC is a tightly associated α_2-dimer, which is the typical fold of the α-family of pyridoxal-5′-phosphate (PLP)-dependent enzymes[12] of which aspartate aminotransferase (AAT)[13] is the prototype[14–16]. Each of the two monomers is composed of three distinct domains (Fig. 2). The structures of two other members of this family with decarboxylase activity have been determined so far: bacterial ornithine decarboxylase (OrnDC)[17] and dialkylglycine decarboxylase (DGD)[18]. The large domain of DDC contains the PLP binding site and consists of a central, seven-stranded mixed β-sheet

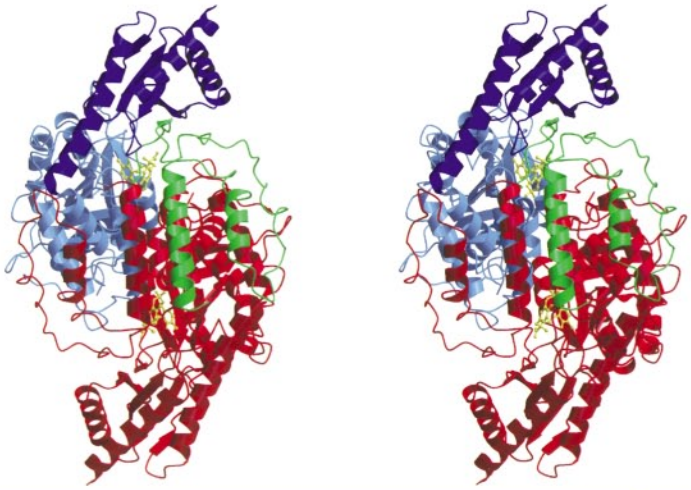

Fig. 2 Stereo view ribbon diagram of the polypeptide backbone of DDC. The view is directly down the two-fold symmetry axis. One monomer is completely red, whereas the other is green (N-terminal domain), cyan (large domain) and blue (small domain). The cofactors (PLP) and the inhibitors (carbiDOPA) are shown in ball-and-stick representation in yellow. The N-terminal domain of one monomer packs on top of the other monomer, resulting in an extended dimer interface. The picture was drawn with MOLSCRIPT[50] and RASTER3D[51].

surrounded by eight α-helices in a typical α/β fold. The C-terminal small domain comprises a four-stranded antiparallel β-sheet with three helices packed against the face opposite the large domain.

In addition to these two domains, found in all enzymes of the α-family, DDC contains an additional N-terminal domain (residues 1–85). This domain is composed of two parallel helices linked by an extended strand. This structure lies like a flap over the top of the second subunit and *vice versa*, with the first helix of one subunit aligning antiparallel to the equivalent helix of the other subunit (Fig. 2). The residues 75–77 of this N-terminal domain together with the residues 433–435 of the small domain form a short two-stranded β-sheet. The N-terminal domain is unlikely to represent an autonomous folding unit but is most likely stable only in the context of the dimer by extending the interface between two monomers (Fig. 2). A similar domain swap was found in DGD, where a shorter N-terminal segment forms a clamp to the neighboring subunit, and an additional four-stranded β-sheet is formed. Although the topologies of the large and the small domains in DDC and in OrnDC are very similar, their N-terminal domains differ significantly, and the C-terminal domain of OrnDC (residues 620–730) is not present in DDC at all. Looking from the N-terminus, structural equivalence between DDC and OrnDC starts from residue 114 within the forth α-helix of DDC, whereas DDC and DGD demonstrate structural equivalence starting from residue 86 within α-helix 3 of DDC.

The active site

The active site of DDC is located near the monomer–monomer interface but is composed mainly of residues from one monomer (Figs 2, 3). In the internal aldimine form of the ligand-free DDC, the cofactor PLP binds to Lys 303 through a Schiff base linkage. The salt bridge between the carboxylate group of Asp 271 and the protonated pyridine nitrogen of the cofactor provides a strong electron sink capable of stabilizing the obligatory carbanionic intermediates[16]. The cofactor, especially its phosphate group, is further anchored to the protein through an extended hydrogen bond network (Fig. 3*b*). The positive pole of the helix dipole from a large domain helix balances the negative charge of the phosphate moiety, in a motif also found in the β-family of PLP-dependent enzymes[19].

The only two active site residues provided by the adjacent monomer, Ile 101′ and Phe 103′, belong to the substrate binding pocket and are in van der Waals contact with the catechol ring of the inhibitor carbiDOPA (Fig. 3*b*). In both structures, the sulfhydryl group of Cys 100′, the residue preceding Ile 101′, is only 4.1 Å apart from that of Cys 111′. Replacement of Cys 111 by an Ala residue[20], as carried out by Dominici *et al.*[20], or formation of a disulfide bridge between these residues would, therefore, perturb the active site geometry and reduce or even abolish enzyme activity.

Inhibitor binding

The inhibitor carbiDOPA binds to the enzyme by forming a hydrazone linkage with the PLP cofactor through its hydrazine moiety, mimicking the external aldimine enzyme–substrate intermediate. The catechol ring of carbiDOPA is deeply buried in the active site cleft and penetrates behind the cofactor ring plane (Fig. 3). The 4′ catechol hydroxyl group of the inhibitor is hydrogen bonded to the hydroxyl group of Thr 82, which is located at the very bottom of the active site cleft. The phosphate group of the cofactor is also involved in substrate binding, because it receives a hydrogen bond from the 3′ catechol hydroxyl group of carbiDOPA. Stacked in front of the cofactor pyridine ring is the imidazole ring of His 192, a highly conserved residue among the sequences of PLP-dependent decarboxylases[21]. Consequently, the same residue is also found in the structure of OrnDC[22], whereas in DGD, this residue is a Trp[23] because this enzyme belongs to the transaminases of the α-family of PLP-dependent enzymes but displays an additional decarboxylase activity. His 192 in DDC forms a hydrogen bond to the carboxylate group of carbiDOPA (Fig. 3*a*). The carboxylate group of the natural substrate L-DOPA is expected to be located even closer to Nε2 atom of His 192 because the carbiDOPA–PLP adduct contains an additional N–N bond, compared to the Schiff base complex with L-DOPA (Fig. 1), and an additional covalent bond between the C=N double bond and its carboxylate group. Therefore,His 192 could play a role in the catalytic mechanism of the enzyme, because the H192A mutant looses catalytic activity completely[21]. This residue could ensure protonation of the quinonoid Cα[16]. However, recent findings than an H192Q mutant of DDC[24] and mutation of the analogous residue (His 167) in glutamate decarboxylase to Asp[25] are still catalytically active rule out such a a function of His 192. Rather, this residue may assist a catalytically active water molecule — or possibly the side chain of Tyr 332 (see below) — which can be accomplished by Asn or Gln residues but not by an Ala. From the structure of DDC, the other His residue, His 302, is shown not to be a catalytic residue as postulated earlier[26]. This has also

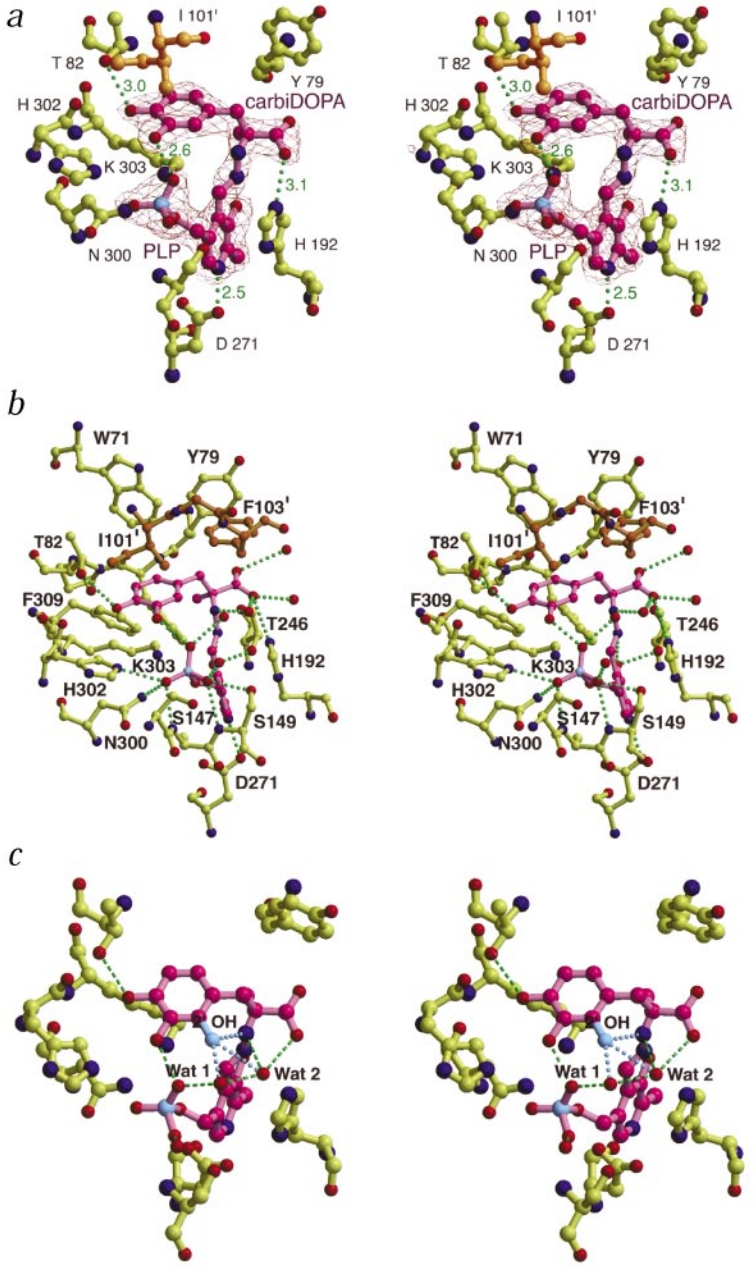

Fig. 3 Active site cleft of DDC in complex with carbiDOPA. ***a***, Stereo view of the electron density of the inhibitor carbiDOPA. The difference electron density ($|F_o| - |F_c|$ map with the inhibitor excluded from the phase calculation) in red, contoured at 4 σ, is superimposed onto the inhibitor model. Nitrogen, phosphate and oxygen atoms are marked blue, cyan and red, respectively. Carbon atoms are colored in yellow for the enzyme, in magenta for the PLP–carbiDOPA complex and in orange for the residues of the other monomer. Hydrogen bonds are indicated in green dotted lines. ***b***, Detailed view of the hydrogen bond interactions, including all structural water molecules in the active site. Color code as in (*a*). ***c***, A model of modified carbiDOPA with an additional 2′ hydroxyl group (cyan). The newly established hydrogen bonds to the structural water molecules and the hydrazone nitrogen are indicated as dotted lines (cyan). Otherwise, the color code is as in (*a*). The picture was drawn with MOLSCRIPT[50] and RASTER3D[51].

been confirmed by the mutation analysis of a H302Q mutant enzyme[24]. Finally, the active site residue Lys 303 presumably displaces the amino group of the product by nucleophilic attack on the imine bond (transaldimination) and, thus, is responsible for product release as shown by the mutation analysis of a K303A mutant[27]. Except for a His residue in front of the cofactor A-face, which has a very similar conformation in both DDC and OrnDC, the remainder of the active site cleft differs considerably in the two enzymes.

According to the model for control of the reaction specificity of PLP-dependent enzymes proposed by Dunathan[28], the scissile bond of the external aldimine intermediate must be oriented perpendicularly to the coenzyme π-bonding system. In this way, the σ–π orbital overlap in the transition state is maximized, leading to an optimized reaction rate. In the structure of the DDC–carbiDOPA complex, the carboxylate moiety of the inhibitor is clearly in an orientation with the Cα–CO_2^- bond approximately orthogonal to the plane of the coenzyme ring (Fig. 3*a*,*b*). This orientation in the real external aldimine intermediate would allow the reaction to take advantage of the stereoelectric effects, which were proposed by Dunathan to play a major role in control of the reaction specificity in PLP-dependent enzymes[28]. The inhibitor complexes of DGD[23] are bound in a conformation as required for transamination rather than decarboxylation. Accordingly, these inhibitors have their carboxylate group not orthogonal to the ring system of the cofactor.

Flexible loop

In the structures of all three crystal forms of DDC, a short stretch of 11 amino acids (residues 328–339) is invisible in the electron density map. These residues belong to a mobile loop that seems to be important for the catalytic mechanism[29,30]. Recombinant DDC lacking this loop was found to be catalytically inactive. Ishii *et al.*[30] have shown that these residues are prone to cleavage by proteases, indicating their flexibility in the ligand-free form of DDC, whereas they are not cleaved in the inhibitor complex of DDC with L-DOPA methyl ester. During catalysis, this loop is expected to adopt a less solvent- and protease-exposed conformation. The loop is located at the dimer interface and possibly extends towards the active site of the other monomer in a closed conformation. In such a conformation, it could occlude the active site cleft from the solvent during catalysis and some loop residues could even take part in the catalytic mechanism.

The active site of DGD is more open and lacks any similar loop protecting or closing down the active site cavity during catalysis. In contrast, in AAT the small domain acts as a hinge in substrate binding and occludes the active site cavity from the solvent to enhance catalysis[31]. In OrnDC, the additional C-terminal domain (residues 569–730) is located close to the active site cavity, with residues 660–664 of this domain being in close proximity of the active site PLP.

Also in other PLP-dependent enzymes, the active site is occluded from the solvent during catalysis either by a mobile loop (as in glutamate 1-semialdehyde aminotransferase)[32] or by a movable subdomain (as in O-acetylserine sulfhydrylase)[33]. A

Table 1 Data collection and phasing statistics

	CarbiDOPA	Native	Ta_6Br_{12}	Native	Ta_6Br_{12} low	Ta_6Br_{12} high
Crystal form	D1	D2	D2	D3	D3	D3
Space group	$P6_2$	$P6_2$	$P6_2$	$P6_422$	$P6_422$	$P6_422$
Unit cell (Å)						
a = b	154.36	152.86	152.66	302.33	304.99	304.07
c	86.78	86.6	86.77	178.08	179.74	178.71
Monomers / au	2	2	2	8	8	8
Soaking concentration	200 mM (carbiDOPA)	–	half saturated (Ta_6Br_{12})	–	saturated (Ta_6Br_{12})	half saturated (Ta_6Br_{12})
Soaking time (h)	24	–	8	–	8	8
Data collection						
Resolution (Å)	2.25	2.6	2.6	2.56	3.65	2.5
Unique reflections	53,622	31,347	63,038	148,258	97,358	247,025
Completeness (%)	95.8	88.4	90.3	97.5	93.7	77.2
R_{sym}[1]	5.6	8.6	10.6	7.6	15.7	12.2
R_{deriv}[2]	–	–	15.9	–	36.3	33.9
Phasing						
Resolution (Å)	–	–	4.1	–	3.65	2.56
Heavy atom sites	–	–	2	–	8	8
R_{Cullis}[3]	–	–	0.91	–	na[4]	0.98
R_{Cullis} anomalous	–	–	0.93	–	0.87	0.83
Phasing power[5]	–	–	0.43	–	na[4]	0.26
Phasing power-anomalous	–	–	0.42	–	0.90	0.69

[1] $R_{sym} = \sum |I - \langle I \rangle| / \sum I$.
[2] $R_{deriv} = \sum ||F_{PH}| - |F_P|| / \sum |F_P|$.
[3] $R_{Cullis} = \sum ||F_{PH}| - |F_P + F_H|| / \sum ||F_{PH}| - |F_P||$.
[4] na = not applicable
[5] Phasing power = $(\sum |F_H|^2 / \sum (|F_{PH}| - |F_P|)^2)^{1/2}$.

similar function of mobile regions in proteins has been demonstrated for several other enzymes, including triosephosphate isomerase[34], tyrosyl-tRNA synthetase[35], glutathionine synthase[36] and ribulose biphosphate carboxylase[37]. In each of these enzymes, several amino acids in the lid are highly conserved and essential for catalytic activity[38]. Also in the flexible loop of DDC are highly conserved residues essential for the catalytic reaction[21]. Tyr 332 is highly conserved, and residue 334 is in most PLP-dependent decarboxylases either as a Lys or an Arg residue[21]. These conserved residues are located in the middle of the flexible loop, which in a closed conformation could place these residues in close proximity to the active site cleft. Because the carboxylate moiety of the inhibitor is solvent exposed in the crystal structure (Fig. 3*b*), Lys 334 may form a hydrogen-bonded ionic interaction with the carboxylate group of the substrates by replacing the two structural water molecules. Because there are no obvious differences between the ligand-free and the complex structures, which could explain such a loop movement, an interaction of some loop residues with the inhibitor itself is likely to cause this conformational change. In such a conformation of the flexible loop, the highly conserved Tyr 332 could also be located close to the substrate. Tyr residues have been shown to act as a proton donor during catalysis[39]; hence, Tyr 332 could act as a possible proton donor for the quinonoid Cα. In agreement with this, the conservative Y332F substitution resulted in a catalytically inactive enzyme[21], an indication that this residue is important for the enzymatic activity of DDC.

Table 2 Model building and refinement

	CarbiDOPA	Native
Crystal form	D1	D2
Resolution (Å)	2.25	2.6
R-factor (%)[1]	14.4	20.5
R_{free} (%)[1]	18.7	25.7
Bond Distances (Å)[2]	0.009	0.009
Bond Angles (°)[2]	1.478	1.418
Number of water molecules	445	95
Average B-factor (Å^2)		
Protein	23.0	33.6
PLP–carbiDOPA	22.2	28.3
Solvent	30.7	28.9

[1] R-factor = $\sum |F_o| - |F_c| / \sum |F_c|$.
[2] R.m.s. error.

Inhibitor design

In the carbiDOPA–inhibitor complex structure, five structural water molecules interact with the cofactor and the inhibitor (Fig. 3*b*). Notably, benserazide has an additional 2′ hydroxyl group on the phenyl ring compared to carbiDOPA (Fig. 1). When adding an analogous hydroxyl group to carbiDOPA in the conformation observed in the crystal structure, this group can form hydrogen bonds to two of these five structural water molecules without shifting their position (Fig. 3*c*). This additional 2′ hydroxyl group explains the strong binding of benserazide to DDC. Furthermore, an additional intramolecular hydrogen bond between this group in carbiDOPA and a nitrogen atom of the hydrazine group can be established. However, this will be a

weaker hydrogen bonding interaction, because the nitrogen is not exactly coplanar with the inhibitor phenyl ring. Therefore, we propose that such a modification of carbiDOPA would improve its binding properties due to these three additional hydrogen bonds.

In summary, the crystal structure of DDC would assist in the design of more potent DDC inhibitors than carbiDOPA or benserazide. Such new drugs with better pharmacological characteristics would allow the reduction of the large dose (up to 1 g d^{-1}) of L-DOPA needed for efficient treatment of PD and, thus, reduce the very undesirable side effects of the drugs most commonly[5] used in its treatment.

Methods

Crystallization. Crystals of form D1 were grown according to Malashkevich *et al.*[11], and crystals of form D3 were grown according to Malashkevich *et al.*[40] Crystals of form D2 were grown in 24-well Limbro plates by vapor diffusion using the hanging-drop method[41]. The 1 ml well solution contained 30% (w/v) polyethylene glycol monomethyl ester (PEG MME) 5000, 50 mM 2-morpholinoethanesulfonic acid (MES)-KOH, pH 6.5, and 400 mM ammonium sulfate. The 4 µl drop contained 2 µl enzyme at a concentration of 30.0 mg ml^{-1} and 2 µl well solution. Crystals grew within one month to a size of $0.5 \times 0.2 \times 0.2$ mm^3. The crystals belong to the hexagonal space group $P6_2$ with unit cell dimensions a = b = 152.65 Å and c = 86.77 Å, and contain one dimer per asymmetric unit, corresponding to a Matthews volume V_M of 2.9 $Å^3$ Da^{-1}.

Data collection, processing and phasing. The X-ray diffraction data sets from the native protein in crystal form D3 and from the Ta_6Br_{12} derivative of crystal form D2 were collected at 100 K on the X11 beam-line (EMBL, DESY Hamburg) at λ = 0.91 Å, close to the absorption edge of bromine (λ = 0.92 Å). The low resolution and the high resolution MAD data sets from the Ta_6Br_{12} derivative of crystal form D3 were collected at 100 K on the X31 beamline (EMBL, DESY Hamburg) and the BW6 beamline (MPG-ASMB, DESY Hamburg), respectively, at a wavelength of λ = 1.25 Å, close to the absorption edge of Ta. Data were processed, integrated and scaled using either DENZO and SCALEPACK[42], or MOSFLM[43] and the CCP4 suite[44]. Initial heavy atom positions were obtained from anomalous difference Patterson maps. Heavy atom parameters were refined using a modified version of SHARP[45], including a cluster refinement procedure. Phasing was further improved by multiple crystal averaging, solvent flattening and histogram matching using DMMULTI from the CCP4 suite[44].

Model building and refinement. The partial initial atomic model was 'automatically' built in the crystal form D1 with wARP[46]. The model was further improved in a cyclic procedure of (i) model building using O[47], (ii) refinement using REFMAC[48] and (iii) multiple crystal averaging using the model phases of the most recently refined model in crystal form D1 with phases obtained from the Ta_6Br_{12} derivatives of the two other crystal forms using DMMULTI[44]. The final model, which was refined using CNS[49] to an R-factor of 14.4% (20.0–2.2 Å) and an R_{free} of 18.7%, comprises one dimer of DDC, two cofactors (PLP), two inhibitors (carbiDOPA), four sulfate ions and 455 water molecules. R.m.s. deviations from ideality in bond lengths and angles are 0.009 Å and 1.478°, respectively (Table 2).

Coordinates. Coordinates have been deposited in the Protein Data Bank (accession codes 1JS6 (ligand-free DDC) and 1JS3 (DDC in complex with carbiDOPA)).

Acknowledgments

Special thanks go to E. De La Fortelle and C. Vonrhein for extremely helpful discussion and to R. Huber, Max-Planck Institut für Biochemie, Martinsried, Germany, for his kind gift of the tantalum cluster.

Correspondence should be addressed to P.B. *email: Peter.Burkhard@unibas.ch*

Received 25 June, 2001; accepted 22 August, 2001.

1. Feany, M.B. & Bender, W.W. *Nature* **404**, 394–398 (2000).
2. Masliah, E. *et al. Science* **287**, 1265–1269 (2000).
3. Aminoff, M.J. *West J. Med.* **161**, 303–308 (1994).
4. Opacka-Juffry, J. & Brooks, D.J. *Mov. Disord.* **10**, 241–249 (1995).
5. Agid, Y., Chase, T. & Marsden, D. *Lancet* **351**, 851–852 (1998).
6. Brannan, T., Prikhojan, A. & Yahr, M.D. *J. Neural Transm.* **103**, 1287–1294 (1996).
7. Kordower, J.H. *et al. Science* **290**, 767–773 (2000).
8. Kang, U.J. *Mov. Disord.* **13**, 59–72 (1998).
9. Diederich, C. *et al. Pharmacology* **55**, 109–116 (1997).
10. Myers, C.S., Witten, M., Yu, Y.L. & Wagner, G.C. *Mol. Chem. Neuropathol.* **33**, 81–97 (1998).
11. Malashkevich, V.N. *et al. J. Mol. Biol.* **224**, 1167–1170 (1992).
12. Alexander, F.W., Sandmeier, E., Mehta, P.K. & Christen, P. *Eur. J. Biochem.* **219**, 953–960 (1994).
13. Ford, G.C., Eichele, G. & Jansonius, J.N. *Proc. Natl. Acad. Sci. USA* **77**, 2559–2563 (1980).
14. John, R.A. *Biochim. Biophys. Acta* **1248**, 81–96 (1995).
15. Schneider, G., Kack, H. & Lindqvist, Y. *Struct. Fold. Des.* **8**, 1–6 (2000).
16. Jansonius, J.N. *Curr. Opin. Strut. Biol.* **8**, 759–769 (1998).
17. Momany, C., Ernst, S., Ghosh, R., Chang, N.L. & Hackert, M.L. *J. Mol. Biol.* **252**, 643–655 (1995).
18. Toney, M.D., Hohenester, E., Cowan, S.W. & Jansonius, J.N. *Science* **261**, 756–759 (1993).
19. Burkhard, P. *et al. J. Mol. Biol.* **283**, 121–133 (1998).
20. Dominici, P., Moore, P.S., Castellani, S., Bertoldi, M. & Voltattorni, C.B. *Protein Sci.* **6**, 2007–2015 (1997).
21. Ishii, S., Mizuguchi, H., Nishino, J., Hayashi, H. & Kagamiyama, H. *J. Biochem. (Tokyo)* **120**, 369–376 (1996).
22. Momany, C., Ghosh, R. & Hackert, M.L. *Protein Sci.* **4**, 849–854 (1995).
23. Malashkevich, V.N., Strop, P., Keller, J.W., Jansonius, J.N. & Toney, M.D. *J. Mol. Biol.* **294**, 193–200 (1999).
24. Bertoldi, M., Castellani, S. & Bori Voltattorni, C. *Eur. J. Biochem.* **268**, 2975–2981 (2001).
25. Tramonti, A., De Biase, D., Giartosio, A., Bossa, F. & John, R.A. *J. Biol. Chem.* **273**, 1939–1945 (1998).
26. Poupon, A. *et al. Proteins* **37**, 191–203 (1999).
27. Nishino, J., Hayashi, H., Ishii, S. & Kagamiyama, H. *J. Biochem. (Tokyo)* **121**, 604–611 (1997).
28. Dunathan, H.C. *Proc. Natl. Acad. Sci. USA* **55**, 712–716 (1966).
29. Bertoldi, M., Frigeri, P., Paci, M. & Voltattorni, C.B. *J. Biol. Chem.* **274**, 5514–5521 (1999).
30. Ishii, S., Hayashi, H., Okamoto, A. & Kagamiyama, H. *Protein Sci.* **7**, 1802–1810 (1998).
31. Kirsch, J.F. *et al. J. Mol. Biol.* **174**, 497–525 (1984).
32. Hennig, M., Grimm, B., Contestabile, R., John, R.A. & Jansonius, J.N. *Proc. Natl. Acad. Sci. USA* **94**, 4866–4871.(1997).
33. Burkhard, P., Tai, C.H., Ristroph, C.M., Cook, P.F. & Jansonius, J.N. *J. Mol. Biol.* **291**, 941–953 (1999).
34. Joseph, D., Petsko, G.A. & Karplus, M. *Science* **249**, 1425–1428 (1990).
35. First, E.A. & Fersht, A.R. *Biochemistry* **32**, 13658–13663 (1993).
36. Kato, H. *et al. Biochemistry* **33**, 4995–4999 (1994).
37. Larson, E.M., Larimer, F.W. & Hartman, F.C. *Biochemistry* **34**, 4531–4537 (1995).
38. Fetrow, J.S. *FASEB J.* **9**, 708–717 (1995).
39. Krupka, H.I., Huber, R., Holt, S.C. & Clausen, T. *EMBO J.* **19**, 3168–3178 (2000).
40. Malashkevich, V.N. *et al. Acta Crystallogr. D* **55**, 568–570 (1999).
41. McPherson, A. *Preparation and analysis of protein crystals.* (John Wiley and Sons, Inc., New York; 1982).
42. Otwinowski, Z. & Minor, W. *Processing of X-ray diffration data collected in oscillation mode.* 307–325 (Academic Press, San Diego; 1997).
43. Leslie, A.G.W. *MOSFLM users guide.* (MRC-LMB, Cambridge UK; 1994).
44. CCP4. *Acta Crystallogr. D* **50**, 760–763 (1994).
45. De La Fortelle, E. & Bricogne, G. *Maximum-likelihood heavy-atom parameter refinement for multiple isomorphous replacement and multiwavelength anomalous diffraction methods.* 472–493 (Academic Press, San Diego; 1997).
46. Perrakis, A., Sixma, T.K., Wilson, K.S. & Lamzin, V.S. *Acta Crystallogr. D* **55**, 448–455 (1997).
47. Jones, T.A., Zou, J.Y., Cowan, S.W. & Kjeldgaard. *Acta Crystallogr. A* **47**, 110–119 (1991).
48. Murshudov, G.N., Vagin, A.A. & Dodson, E.J. *Acta Crystallogr. D* **53**, 240–255 (1997).
49. Brünger, A.T. *et al. Acta Crystallogr D* **54**, 905–921 (1998).
50. Kraulis, P.J. *J. Appl. Crystallogr.* **24**, 946–950 (1991).
51. Merritt, E.A. & Bacon, D.J. RASTER3D: *Photorealistic molecular graphics.* 505–524 (Academic Press, San Diego; 1997).